

# Fractional modeling for enhancing the thermal performance of conventional solar still using hybrid nanofluid: Energy and exergy analysis

E.F. El-Gazar<sup>a,b,\*</sup>, W.K. Zahra<sup>a,c</sup>, Hamdy Hassan<sup>d,e</sup>, Sherif I. Rabia<sup>a,f</sup>

<sup>a</sup> Department of Mathematics, Institute of Basic and Applied Sciences, Egypt-Japan University of Science and Technology (E-JUST), New Borg El-Arab City, Alexandria, Egypt

<sup>b</sup> Basic Science Department, Benha Faculty of Engineering, Benha University, Benha, Egypt

<sup>c</sup> Department of Engineering Physics and Mathematics, Faculty of Engineering, Tanta University, Tanta, Egypt

<sup>d</sup> Energy Resources Engineering Department, Egypt - Japan University of Science and Technology (E-JUST), Alexandria, Egypt

<sup>e</sup> Mechanical Engineering Department, Faculty of Engineering, Assiut University, Assiut, Egypt

<sup>f</sup> Department of Engineering Mathematics and Physics, Faculty of Engineering, Alexandria University, Alexandria, Egypt

## HIGHLIGHTS

- A fractional model for the performance of the solar still system using hybrid nanofluid.
- The error of the fractional model due to the experimental data is 3.243% compared to 20.08% for the classical one.
- Hybrid nanofluid rises daily productivity by 27.2% in summer and 21.7%, in winter compared with still without nanofluid.
- Hybrid nano rises the average energy efficiency by 12.6% in summer and 13.4% in winter.
- Hybrid nano rises the average exergy efficiency by 22.5% in summer and 13.4% in winter.

## ARTICLE INFO

### Keywords:

Fractional model  
Solar still  
Hybrid nano  
Productivity  
Energy  
Exergy

## ABSTRACT

A novel fractional model based on the Riemann Liouville fractional derivative to simulate the thermal performance of conventional solar still and show the effect of using hybrid nanofluid on the desalination system is presented. The results of the fractional model are compared with the results obtained from the classical model, then compared to real experimental data under various climate conditions of Upper Egypt. The theoretical results reveal a perfect agreement between the proposed fractional model and the experimental data of the still with a percentage of error reached 1.486% in summer and 3.243% in winter compared to an error percentage of 24.1% and 20.08%, in case of applying the classical. Moreover, the performance of the modified solar still after adding hybrid nanoparticles is also compared with the conventional solar still. The model is implemented using a hybrid nanofluid of alumina and copper oxide ( $Al_2O_3-CuO$ ) with a concentration of 0.025% for each nanoparticle. The results show that using hybrid nanofluid raises the still daily productivity to 5.5239 kg/m<sup>2</sup>-day in summer and 3.1079 kg/m<sup>2</sup>-day in winter of an enhancement in the still output yield of 27.2% and 21.7% compared with still without nanoparticles. The average energy efficiency of the still in summer is also increased to 49.54% and 23.212% in summer and winter, respectively, with an augmentation of 12.6% and 11.85% in hot and cold climate conditions, respectively. In addition, the average exergy efficiency is raised by 22.5% in summer and 13.4% in winter by using hybrid nano.

## 1. Introduction

The shortage of freshwater is considered one of the most critical

issues that threaten humanity; however, the sources of fresh water on our planet are limited. About 97% of the water on the Earth is brackish water, which is coming from oceans and seas, while only 3% of the available water on our planet is fresh water and, two-thirds of this

\* Corresponding author at: Department of Mathematics, Institute of Basic and Applied Sciences, Egypt-Japan University of Science and Technology (E-JUST), New Borg El-Arab City, Alexandria, Egypt.

E-mail addresses: [eman.elgazar@ejust.edu.eg](mailto:eman.elgazar@ejust.edu.eg) (E.F. El-Gazar), [waheed.zahra@ejust.edu.eg](mailto:waheed.zahra@ejust.edu.eg) (W.K. Zahra), [hamdy.aboali@ejust.edu.eg](mailto:hamdy.aboali@ejust.edu.eg) (H. Hassan), [sherif.rabia@ejust.edu.eg](mailto:sherif.rabia@ejust.edu.eg) (S.I. Rabia).

<https://doi.org/10.1016/j.desal.2020.114847>

Received 22 June 2020; Received in revised form 4 November 2020; Accepted 6 November 2020

Available online 19 January 2021

0011-9164/© 2020 Elsevier B.V. All rights reserved.

percentage in frozen glaciers or in remote mountain regions that are covered with ice. So, the accessibility of getting healthy freshwater from

### Nomenclatures

|     |   |
|-----|---|
| A   | Area in $m^2$                                   |
| C   | Specific heat in $J/kg \cdot K$                 |
| $h$ | Coefficient of heat transfer in $W/m^2 \cdot K$ |
| I   | Incident solar irradiance in $W/m^2$            |
| K   | Thermal conductivity in $W/m \cdot K$           |
| $m$ | Mass in kg                                      |
| T   | Temperature in $^{\circ}C$                      |

### Greek symbols

|           |  |
|-----------|--|
| $\eta$    | Efficiency of the solar still                  |
| $\Phi$    | Volume fractional                              |
| $\rho$    | Density in $kg/m^3$                            |
| $\mu$     | Viscosity                                      |
| $\lambda$ | Latent heat of evaporation of water ( $J/kg$ ) |

### Subscripts

|    |              |
|----|--------------|
| a  | Ambient      |
| ex | Exergy       |
| g  | Glass        |
| hf | Hybrid fluid |
| p  | Plate        |
| th | Thermal      |
| w  | Water        |
| s  | Sky          |

these regions or seas is one of the critical difficulties that threaten the world [1]. As a result of the population growth and the increase in the demands of water consumption for drinking, domestic use, food production, agriculture, industrials, and many other purposes, it is predicted that about one-quarter of the population of the earth will suffer from the shortage of fresh water by the year 2030 [2,3]. So, to overcome this problem and the high demand for water due to the growing population, it was essential for people to depend on the resources of saline water either from seas or oceans to get on pure water through the process of desalination [4]. Many systems related to the desalination process have been carried out and developed in the last few years. One of these systems is the conventional solar still (SS), which is used to desalinate the salty water to obtain drinkable freshwater by using solar energy. In general, the basic concept of using solar still is very simple, with a low initial cost. The saline water lying in a closed enclosure then, it is evaporated by using the sunbeams. After that, the water vapor is condensed on the glass cover surface. Finally, fresh water is collected in tanks for use [5].

The considerable problem of the SS system is the lower yield of the water produced, which reaches nearly 2.5 to 5  $L/m^2$  per day. To overcome this problem, many experimental and some theoretical studies have been done to increase its productivity and efficiency. Some of these works focused on adding some materials to enhance the performance of the conventional SS; for example, Sathyamurthy and Nagarajan [6] experimentally used sand heat energy storage to increase the water productivity from about 2 to 5  $kg/m^2 \cdot day$ . Shalaby et al. [7] experimentally suggested a modified system using a V-corrugated designed absorber plate, which led to an increase of about 12% with respect to the traditional unit. Panchal et al. [8] implemented an experimental study on a double SS coupled with evacuated tubes and solid fins with 2.5 cm and 3 cm depth of salty water in the still basin. The findings revealed that by adding the solid fins in the double SS, the output of the still was increased by 25% compared with the conventional double basin SS with

evacuated tubes. Elashmawy [9] presented an experimental investigation on the influence of using material of gravel on the performance of tubular SS integrated with a parabolic solar tracking system. The results show an increase in the rate of water productivity reached to 4.51  $L/m^2 \cdot day$  and an improvement in the efficiency of 36.34%. Moreover, Naroei et al. [10] introduced a numerical and experimental study of photovoltaic thermal (PVT) collector connected to stepped SS. They proved that the connection between the PVT collector to the stepped SS helps in enhancing the freshwater productivity by about 20%, and the PV collector could supply around 1060 W/day of electrical power during the sunshine days for use in other purposes. Another experiment was carried out by H.hassan et al. [11] to investigate the exergy and energy analysis of solar desalination system coupled with a photovoltaic module. This integration between the SS system and PV enhances the energy and exergy efficiency of SS by about 10% and 30.72%, respectively. Panchal and Sathyamurthi [12] investigated the thermal performance of conventional SS integrating with porous fins. The results found that adding the fins increased the freshwater productivity to reach 3.8 L comparing with 2.67 L from the conventional SS, which means an improvement in the still output yield by 42.3%. A recent study to enhance the productivity of the SS system was investigated in [13]; the study based on using single-slope SS supplied with a thermoelectric module as a heater operated by a photovoltaic panel. They show that there was an enhancement in the still efficiency reached to about 27.8%.

Another way for improving the productivity of the SS is by using nanofluid which means mixing nanoparticles in the basic fluid (saline water). The nanoparticles help in improving the thermal conductivity and hence the heat transfer, which leads to an increase in the evaporation rate and, hence increasing the still productivity. For example, nanoparticle plays a significant effect in improving the emission and combustion behavior for diesel and biodiesel blends [14]. The performance of the diesel engine after using SC1 (supramolecular complex) nanofluid enhanced the efficiency of the thermal brake by about 14.8–20.52%. A review to show the effect of using different types of nanoparticles on the thermal and electrical performance of photovoltaic system PV/T was also discussed in [15]. According to the literature, many experimental and numerical studies had been done in the last years to show the performance of the SS system by using various kinds of nanoparticles of various shapes and sizes. It was observed that there were positive effects in improving the SS performance because of the large thermal conductivity for most of these nanoparticles. Panchal et al. [16] implemented an experimental study to investigate the effect of using Magnesium Oxide (MgO) and Titanium dioxide ( $TiO_2$ ) as nanoparticles on the productivity of stepped SS. The experiment is performed with different concentrations of nanoparticles from 0.1 to 0.2%. The results found that the still productivity was raised by about 45.8% and 20.4% using MgO and  $TiO_2$  respectively at a concentration of 0.2%. It was also observed that the nanoparticles were stable for nearly three months when using a concentration of 0.2%. Another experimental work on a stepped SS was carried out by Sathyamurthy et al. [17] aims to calculate the amount of freshwater production after using  $TiO_2$  and MgO of nanoparticles. The results show an enhancement in the heat transfer coefficient of the evaporation rate, and hence, an improvement in the freshwater yield reached about 4.5  $kg/m^2$  using  $TiO_2$  and 2.7  $kg/m^2$  using MgO. Kabeel et al. [18] presented a new experimental study to show the impact of coating the basin of SS with  $TiO_2$  black paint nanoparticles. The experiment was done under various water depths ranged from 1 cm to 3.5 cm, with an area of 0.25  $m^2$  for the absorber plate. The findings revealed an improvement in water temperature by 1.5–2.2  $^{\circ}C$  and an increase in the maximum hourly productivity by 0.6 kg after coating the absorber plate with the nanoparticle. Kabeel et al. [19] performed experimental modifications on the conventional SS, to show the impacts of using various nanoparticles on the thermal performance of conventional SS. The results showed that the rate of water productivity was increased due to using aluminum oxide ( $Al_2O_3$ ) and cuprous oxide ( $Cu_2O$ ) nanoparticles during the daytime. Gupta et al.

**Table 1**

The literature studies which summarize the existing nanofluids with the SS system.

| Reference            | Type of nanofluid                                    | The concentration of nanofluid (%) | Type of SS                                   | Main output  |
|----------------------|--|------------------------------------|--|--|
| Kabeel et al. [19]   | Al <sub>2</sub> O <sub>3</sub> and Cu <sub>2</sub> O | 0.2                                | Conventional SS with vacuum fan.             | The still productivity increased by 88.97% and 93.87% for Al <sub>2</sub> O <sub>3</sub> and Cu <sub>2</sub> O, respectively.  |
| Gupta et al. [20]    | CuO  | 0.12                               | Passive SS                                   | The productivity of still reached to 3.058 kg/m <sup>2</sup> -day  |
| Parsa et al. [21]    | Silver nanoparticles                                 | 0.04                               | Conventional SS at the peak of the mountain. | The values of energy and exergy efficiency increased by 55.98% and 9.27%, respectively.  |
| Sahota et al. [22]   | MWCNTs and Al <sub>2</sub> O <sub>3</sub>            | 0.04, 0.08, and 0.12               | Passive double slope SS.                     | Al <sub>2</sub> O <sub>3</sub> raises the evaporative and convective rate by 42.6% and 52.1%, respectively. While MWCNT raises the evaporative and convective rate by 65.3% and 58.1%. |
| Kabeel et al. [23]   | Cu <sub>2</sub> O                                    | Range from 0.02 to 0.3             | SS with an external condenser.               | The daily efficiency of the still was 84.16% and 73.85% with using Cu <sub>2</sub> O and Al <sub>2</sub> O <sub>3</sub> , respectively   |
| Rashidi et al. [24]  | Al <sub>2</sub> O <sub>3</sub>                       | Range from 0 to 5                  | Cascade SS                                   | Enhancement in water productivity with 22%   |
| Rashidi et al. [26]  | Al <sub>2</sub> O <sub>3</sub>                       | Range from 0 to 5.                 | Single slope SS                              | Productivity increased by about 25%  |
| Subhedar et al. [28] | Al <sub>2</sub> O <sub>3</sub>                       | 0.05 and 0.1                       | Passive SS with PTC                          | The productivity and efficiency raised to nearly 66% and 70%, respectively   |

[20] implemented an experiment work to show the effect of adding copper oxide (CuO) nanoparticle in a conventional SS at different water depths. It was observed that the amount of water productivity for the modified SS was 3058 mL/m<sup>2</sup> at a water depth of 10 cm and 3445 mL/m<sup>2</sup> at 5 cm per day. Another recent experimental study was implemented by Parsa et al. [21] at the top of a mountain to compare the performance of SS with and without using nanofluid. The experiment based on using nanoparticles of silver and the results found that the SS energy and exergy efficiency was improved by nearly 106% and 196%, respectively. Moreover, Sahota et al. [22] studied the effect of using aluminum oxide (Al<sub>2</sub>O<sub>3</sub>) and multi-wall carbon nanotube (MWCNT) as nanoparticles on the thermophysical characteristics of double slope SS. They found an increase in the temperature difference between nanofluid

and base fluid by around 2 °C–3 °C with using the nanoparticles. Kabeel et al. [23] presented a numerical study to show the effect of using external condensers and nanofluids on the efficiency of the SS. The mathematical modeling is based on fourth-order Runge–Kutta method (RK4), then experimental published data were compared with the simulation results. It was found that the SS efficiency during the day of the modified SS after using various types of nanoparticles, such as Al<sub>2</sub>O<sub>3</sub> reached about 73% by using a fan. Rashidi et al. [24] carried out a numerical study to investigate the effect of using nanofluids on the performance of the cascade SS. All the simulation results have been done using ANSYS software. The results found that by increasing the concentration of the nanoparticles to 5%, the hourly variations in water productivity is increased to nearly 22%. In another study, Al-harahsheh et al. [25] experimentally considered the impact of using a phase change material (PCM) storage unit on the freshwater yield of SS with the aid of solar water collectors. Another theoretical model was proposed by Rashidi et al. [26] to show the influence of using different solid volume fraction of nanoparticles on the freshwater productivity of the conventional SS. This numerical model was developed using Ansys-Fluent software. The numerical results revealed that there was an improvement in the amount of potable water produced from the SS by about 25%. A review to investigate the role of using nanofluids in the desalination process was made by Bait and Ameer [27]. Furthermore, Subhedar et al. [28] used aluminum oxide Al<sub>2</sub>O<sub>3</sub> nanofluid with 0.05% and 0.1% volume fraction for investigating the performance of conventional SS combined with parabolic trough collector (PTC). The results reveal that the single slope SS efficiency raised to 66% and 70% at different concentrations of the nanoparticles. All the previous results related to the SS with nanofluid have been summarized in Table 1.

Recently, researchers have concentrated on using hybrid nanofluids despite single nanofluid in enhancing the performance of solar systems. Hybrid nanofluids mean mixing the base fluid with two types of solid-sized nanoparticles. These kinds of nanoparticles modify the characteristics of heat transfer, change the evaporative rate for base fluid, and hence improve the performance of a solar energy system. The hybrid nanoparticles are used to solve the defect that results from using a single nanoparticle, such as the higher viscosity of a single nanofluid. Based on the work presented by Tayyab and Hafiz [29], hybrid nanofluids proved their efficiency in different applications especially related to solar energy systems. For example, Xiaoke et al. [30] focused on using SiC-MWCNT hybrid nanofluid to study the stability, solar-thermal conversion efficiency, and optical properties for direct absorption solar collector (DASC). The results displayed excellent stability and an increase in conversion efficiency by 48.6%. Vakaa et al. [31] studied the effect of using hybrid nanoparticles of Graphene oxide (GO) and Titanium (TiO<sub>2</sub>) in the application of thermal energy storage. It was observed that by adding of 0.05% of hybrid nanoparticles, there was an improvement in the specific heat by 19.6% compared with using one nanoparticle at the same concentration, and the thermal stability of the new hybrid nanofluid of (GO/TiO<sub>2</sub>) was at a high temperature of 580 °C. An overview of the thermal performance of heat pipe using hybrid nanoparticles was presented in [32]. It was found that using hybrid nanoparticles in the base fluid of heat pipe at a concentration of 1% enhanced heat flux, heat transfer coefficient, and the thermophysical properties of the working medium. Furthermore, many studies in [33–35] have been investigated to show the effect of using hybrid nanofluids in improving the performance of different kinds of solar collectors. Due to the importance of the solar still system and lack of performant presented mathematical modeling that enables to enhance the still performance, it is necessary to find a new way of modeling this system based on the fractional calculus. Modeling utilizing property in various complex systems, dissimilar the classical derivative, where the fractional derivative does not consider only the local characteristics of the physical process dynamics but also it takes into account the global system evolution. Classical calculus is not always precise, and the error between the theoretical and the real experiment results is usually high. So, recent studies have shown that

fractional calculus is the best tool for modeling in different fields of both engineering and science due to its intrinsic and nonlocality nature [26].

In recent years, the field of fractional calculus attracted a lot of mathematicians and proved its efficiency in many numbers of applications such as control engineering, signal processing, image processing, communication, probability theory, biology, chemistry, and heat transfer [36–43]. There are several descriptions of fractional derivatives, such as Caputo and Riemann-Liouville fractional derivatives [44], Caputo-Fabrizio fractional derivative [45], Atangana-Baleanu fractional derivatives [46]. Also, another definition of the fractional derivative which well-suited with the ordinary derivative named Conformable fractional, was introduced by Khalil [47].

Many authors [34–37,39,48,51] have developed analytical and numerical techniques for solving nonlinear unsteady fractional-reaction-diffusion equations with both distributed and constant order derivatives. Sierociuk et al. [52] studied the diffusion process that enables to model heat dissipation in the form of fractional differential equations using different boundary and initial conditions. Furthermore, Zahra et al. [53] introduced a new fractional model for modeling the process of laser drilling using the meshless method. The results of the proposed fractional model show a perfect matching with the experimental data.

Based on the literature survey, it is found that there are a few works that have been presented on the theoretical modeling of solar still compared to the large presented experimental works despite the importance of theoretical work to develop the solar still performance and optimize its working conditions. So, this work focused on solving two significant problems; firstly, most of the presented theoretical models of solar still have been solved using classical derivatives, which produce a significant error in the results compared to the real experimental data. As a result, a fractional model based on the Riemann-Liouville fractional derivative is presented to simulate the thermal behavior of the solar still system and give more accurate results to the experimental work. Secondly, due to the lower productivity for the conventional SS (based on the proposed non-local model), the hybrid nanoparticles are mixed within the saline water (hybrid nanofluid) in the still basin to enhance the process of heat transfer with the saline water. Hence, it improves the thermal performance (temperatures, water productivity, energy efficiency, and exergy efficiency) of the conventional still, then raises its output yield. The model is performed under cold and hot climate conditions in the city of Sohag, Egypt. The advantages of the present work can be summarized as: (i) The fractional model gives an accurate result and a perfect consistency to the experimental data comparing with the classical model. (ii) The new non-local model decreases the percentage of error between the experimental and numerical results. (iii) Hybrid nanoparticles improve the thermophysical properties of the traditional fluid and hence, increase the water productivity of solar still as will be seen later. (iv) Moreover, the hybrid nanofluid helps in raising the energy and exergy efficiency of the conventional solar still.

## 2. Mathematical model

### 2.1. Basic definitions

Different and necessary definitions for the fractional derivatives are introduced in [49,50,54–56] as follows:

**Definition 1.** The Riemann Liouville derivative (RL) of  $T(t)$  is

$${}^{RL}_0 D_t^\alpha T(t) = \frac{1}{\Gamma(n-\alpha)} \frac{d^n}{dt^n} \int_0^t (t-\tau)^{n-\alpha-1} T(\tau) d\tau, n-1 < \alpha \leq n, \quad (1)$$

where  $\Gamma(\cdot)$  is defined as:

$$\Gamma(p) = \int_0^\infty e^{-x} x^{p-1} dx.$$

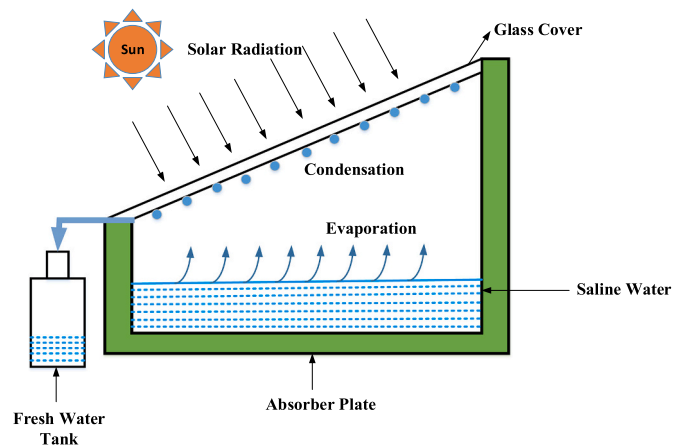


Fig. 1. Schematic diagram for conventional solar still device.

**Definition 2.** The Caputo derivative of  $T(t)$  is

$${}^C_0 D_t^\alpha T(t) = \frac{1}{\Gamma(n-\alpha)} \int_0^t (t-\tau)^{n-\alpha-1} T(\tau) d\tau, n-1 < \alpha \leq n, \quad (2)$$

**Definition 3.** The Grünwald-Letnikov derivative (GL) of  $T(t)$  is

$${}^{GL}_0 D_t^\alpha T(t) = \lim_{h \rightarrow 0} h^{-\alpha} \sum_{j=0}^{[n]} w_j^\alpha T(t-jh), nh = t-a, \alpha > 0, \quad (3)$$

where  $[n]$  is the integer part of  $n$  and the coefficients  $w_j^\alpha$  can be evaluated by

$$w_0^\alpha = 1, w_j^\alpha = \left(1 - \frac{\alpha+1}{j}\right) w_{j-1}^\alpha, j = 1, 2, 3, \dots,$$

Also, the coefficients of the GL fractional derivative satisfy the following:

$$w_0^\alpha = 1, w_1^\alpha = -\alpha, w_2^\alpha \leq w_3^\alpha \leq w_4^\alpha \leq \dots \leq 0, \sum_{j=0}^\infty w_j^\alpha = 0, \sum_{j=0}^n w_j^\alpha \geq 0, n \geq 1.$$

The GL and the RL fractional derivatives are equivalent, while this is not true in the case of the RL and Caputo fractional derivatives unless the initial conditions are zero. Then the RL fractional derivative can be approximated as

$${}^{RL}_0 D_t^\alpha T(t) = h^{-\alpha} \sum_{j=0}^k w_j^\alpha T(t-jh) + O(h) \quad (4)$$

**Definition 4.** The nonstandard GL fractional derivative of  $T(t)$  is

$${}^a_{GL} D_t^\alpha T(t) = \lim_{h \rightarrow 0} \varphi(h)^{-\alpha} \sum_{j=0}^{[n]} w_j^\alpha T(t-jh), \alpha > 0, \quad (5)$$

where  $\varphi(h)$  is a continuous function of step size  $h$  that satisfies:

$$\varphi(h) = h + O(h^2), \text{ and } \varphi(h) \text{ may take one of } h, 1 - e^{-h}, \sinh h \text{ or } \sin h.$$

### 2.2. Solar still model

The thermal model of the conventional SS depicted in Fig. 1 is resulting from the energy balance equations of its three elements (brackish water, glass cover, and absorber plate). The energy balance equations of each part of the solar still are derived from the average temperature in that part. According to the assumptions listed in [1], the energy balance equations can be described as

### 2.2.1. Glass cover

The energy from the inner glass cover is equivalent to the summation of energy losses by radiation and convection heat transfer between the sky and the glass. Then the energy balance equation of the inner glass cover is written as:

$$I(t) \alpha_{\text{eff},g} A_g + h_2 A_w (T_w - T_g) = h_{c_g-a} A_g (T_g - T_a) + h_{r_g-s} A_g (T_g - T_s) + m_g c_g ({}^{\text{RL}}D_t^\alpha T_g), \quad (6)$$

where  ${}^{\text{RL}}D_t^\alpha$  is an RL fractional operator,  $T_g$ , and  $T_w$  are the glass and water temperatures in K, while  $T_a$  is the ambient temperature and  $T_s$  is the sky temperature in K.  $m_g$  and  $c_g$  are the mass in kg and specific heat of the cover respectively in J/kg·K.  $h_{r_g-s}$  and  $h_{c_g-a}$  are radiation and convection heat transfer coefficients, respectively from glass to ambient respectively in W/m<sup>2</sup>·K.

$$h_2 = h_{c_w-g} + h_{e_w-g} + h_{r_w-g}, \quad (7)$$

also,  $h_{c_w-g}$ ,  $h_{r_w-g}$ , and  $h_{e_w-g}$  are evaporative, radiative, and convective heat transfer coefficients, respectively in W/m<sup>2</sup>·K.

### 2.2.2. Brackish water

The energy from the brackish water in the SS is equivalent to the summation of the energy moved out from the saline water to the glass by convection, radiation, and evaporation. Then applying the balance equation, we have

$$I(t) \alpha_{\text{eff},w} A_w + h_1 A_p (T_p - T_w) = h_2 A_w (T_w - T_g) + m_w c_w ({}^{\text{RL}}D_t^\alpha T_w), \quad (8)$$

where  $m_w$  and  $c_w$  are the mass in kg and specific heat in J/kg·K of salty water. The following equation gives the heat transfer coefficient between the water and the absorber plate:

$$h_1 = 0.54 \frac{k_w G_r p r^{0.25}}{x}, \quad (9)$$

where  $k_w$  is the water thermal conductivity in W/m·K,  $G_r$  is the Grashof number, and  $x$  is the characteristic length in m.

### 2.2.3. Absorber plate

The energy from the plate is equal to the summation of energy moved out by convection heat transfer between the plate, the saline water, and energy losses to the air, in addition to the energy accumulation within the absorber plate. This leads to

$$I(t) \alpha_{\text{eff},p} A_p = h_1 A_p (T_p - T_w) + U_b A_p (T_p - T_a) + m_p c_p ({}^{\text{RL}}D_t^\alpha T_p), \quad (10)$$

where  $m_p$  and  $c_p$  are the mass in kg and absorber plate capacity in J/kg·K, and  $U_b$  is the overall coefficient of heat transfer in W/m<sup>2</sup>·K from the basin to the ambient.

### 2.2.4. Water productivity

The formula of the hourly output from the passive solar still  $\dot{m}_{ew}$  is expressed as follows:

$$\dot{m}_{ew} = \frac{h_{ew} A_w (T_w - T_g)}{h_{fg}} \times 3600, \quad (11)$$

where  $h_{ew}$  is the evaporation coefficient of heat transfer in W/m<sup>2</sup>·K between the water and the glass cover, and can be calculated as:

$$h_{ew} = 0.01623 h_{c_w-g} \left[ \frac{P_w - P_g}{T_w - T_g} \right], \quad (12)$$

and  $h_{fg}$  is the latent heat of vaporization of water and is given by:

$$h_{fg} = 2.4935 [10^6 - 947.79 T_i + 0.13132 T_i^2 - 0.00479747 T_i^3], \quad (13)$$

$$\text{and } T_i = \frac{T_w + T_g}{2}.$$

## 2.3. Solar still efficiencies

### 2.3.1. Energy efficiency

The efficiency of the conventional SS is calculated by [5,11,57,58]:

$$\eta_{th} = \frac{\sum P_d \times \lambda_{fg}}{A_p \times \sum I_d(t) \times 3600}, \quad (14)$$

where  $\lambda_{fg}$  is water latent heat of vaporization in J/kg,  $P_d$  is the collected freshwater in m<sup>3</sup>/h,  $A_p$  is the SS area in m<sup>2</sup>, and  $I_d$  is the falling solar energy irradiance in W/m<sup>2</sup>.

### 2.3.2. Exergy efficiency

The exergy analysis utilizes the conservation of both energy and mass principles [1]. The exergy efficiency  $\eta_{ex}$  is the highest work that produced from the system and can be calculated as the ratio of the output exergy of the evaporated salty water  $\dot{E}_{x,out}$  to the input exergy of solar energy  $\dot{E}_{x,in}$  as follows [59,60].

$$\eta_{ex} = \frac{E_{x,out}}{E_{x,in}} = \frac{E_{x,ev}}{E_{x,sun}}, \quad (15)$$

where

$$E_{x,ev} = h_{ew} A_w (T_w - T_g) \left( 1 - \frac{T_a}{T_w} \right), \quad (16)$$

and

$$E_{x,sun} = A_g I(t) \left[ 1 - \frac{4}{3} \left( \frac{T_a}{6000} \right) + \frac{1}{3} \left( \frac{T_a}{6000} \right)^4 \right], \quad (17)$$

where  $T_g$ ,  $T_w$ , and  $T_a$  are the glass, water, and ambient temperature, respectively in K.

## 2.4. Hybrid nanofluid model

One of the most significant techniques used to improve the heat transfer process is by adding nanoparticles which have high thermal conductivity such as Copper Oxide, Alumina, Graphite, and Carbon Nanotubes in fluids.

It is well known that stability is a necessary and sufficient condition for the applications of nanofluids in solar energy systems. The stability of used nanofluids, alumina (Al<sub>2</sub>O<sub>3</sub>) nanofluid is illustrated as described in [61,62]. In this work, the authors investigated the processes of clustering and agglomeration on the three samples of alumina after 3 and 60 days. The results show that by adding the material of surfactant with concentrations of 0.003%, the problem of stability is solved with low dispersion and suspension for 60 days. While, the stability of the copper oxide (CuO) is studied as described in [63], and the results found that, in the presence of surfactant at a concentration of 0.05%, the sample was stable for one month, and the material of surfactant is an economical and easy way to enhance the stability of nanofluids in many systems.

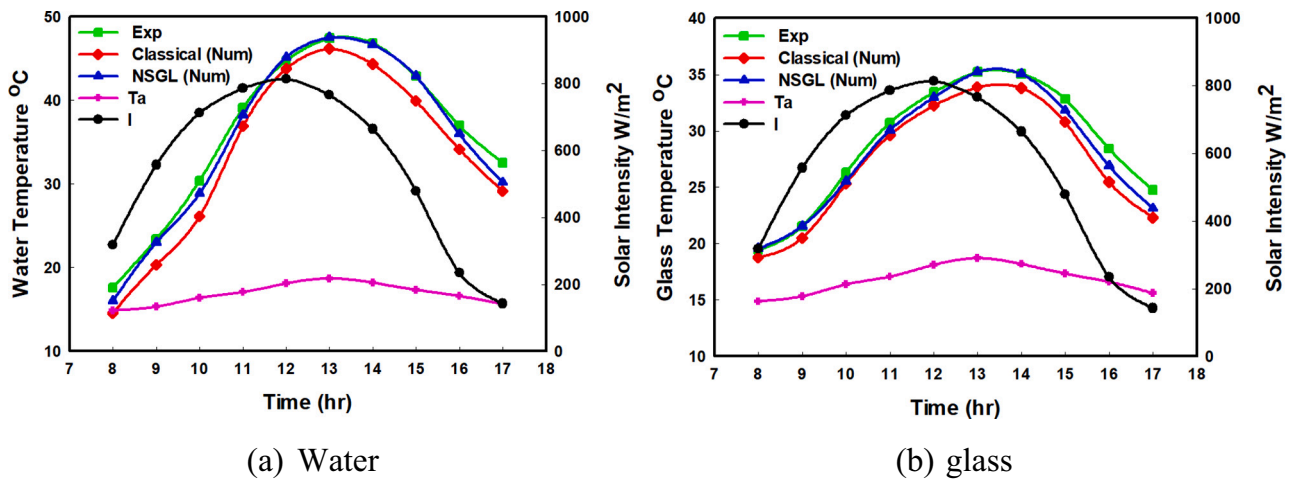


Fig. 2. Hourly variation of water and glass temperatures for classical derivative, NSGL, and experimental in winter.

2.4.1. Thermal conductivity

The most common relation that describes the conductivity of conventional nanofluid depend on the Maxwell–Garnetts (MG) model for the size particles in micrometer [64] [65], is given by

$$K_{nf} = \left[ \frac{K_p + 2K_{bf} - 2\phi(K_{bf} - K_p)}{K_p + 2K_{bf} + \phi(K_{bf} - K_p)} K_{bf} \right], \quad (18)$$

where  $\phi$  is the volume fraction of the particle,  $K_p$ ,  $K_{bf}$ , and  $K_{nf}$  are the thermal conductivities of nanoparticles, base fluid, and nanofluid, respectively in W/m.K. In the case of hybrid nanofluids, the previous relation is modified to

$$K_{hf} = \left[ \frac{(\phi_{Al_2O_3} K_{Al_2O_3} + \phi_{Cu} K_{Cu})(1 + 2\phi_{hf}) + 2K_{bf}\phi_{hf}(1 - \phi_{hf})}{(\phi_{Al_2O_3} K_{Al_2O_3} + \phi_{Cu} K_{Cu})(1 - \phi_{hf}) + 2K_{bf}\phi_{hf}(1 - \phi_{hf})} K_{bf} \right], \quad (19)$$

where  $\phi_{hf}$  is the volume fraction for hybrid nanofluid such that  $\phi_{hf} = \phi_{Al_2O_3} + \phi_{Cu}$ , and  $K_{hf}$  is the hybrid nanofluid thermal conductivity.

2.4.2. Density

The effective density of the applied nanofluid is described [66,67] by

$$\rho_{nf} = (1 - \phi)\rho_{bf} + \phi\rho_p, \quad (20)$$

where  $\rho_{nf}$  is the density of nanofluid,  $\rho_{bf}$ , and  $\rho_p$  are densities of base fluid and nanoparticles, respectively in kg/m<sup>3</sup>. To calculate the density in the case of the hybrid nanofluid, Eq. (20) is modified to

$$\rho_{hf} = (1 - \phi_{hf})\rho_{bf} + \phi_{Al_2O_3}\rho_{Al_2O_3} + \phi_{Cu}\rho_{Cu}, \quad (21)$$

where  $\rho_{hf}$  is the density but for hybrid nanofluid,  $\rho_{Al_2O_3}$ , and  $\rho_{Cu}$  are densities of the Alumina and the Copper oxide nanoparticles, respectively in kg/m<sup>3</sup>.

2.4.3. Specific heat

The specific heat for the nanofluid [68] is given by

$$(C_p)_{nf} = \frac{(1 - \phi)(\rho C_p)_{bf} + \phi(\rho C_p)_p}{\rho_{nf}}, \quad (22)$$

where  $(C_p)_{nf}$  is the heat capacitance of the nanofluid and  $C_p$  is the heat capacitance of nanoparticle in J/kg.K. The previous relation can be modified to compute the specific heat  $(C_p)_{hf}$  for the hybrid nanofluid as follows:

$$(C_p)_{hf} = \frac{(1 - \phi_{hf})(\rho C_p)_{bf} + \phi_{Al_2O_3}(\rho C_p)_{Al_2O_3} + \phi_{Cu}(\rho C_p)_{Cu}}{\rho_{hf}}. \quad (23)$$

2.4.4. Viscosity

The final property that will be used in our model is the viscosity of the nanofluid which can be calculated based on Batchelor’s relation [69] as

$$\mu_{nf} = \frac{\mu_f}{[1 - \phi]^{2.5}}, \quad (24)$$

while the viscosity of the hybrid nanofluid is

$$\mu_{hf} = \frac{\mu_f}{[1 - (\phi_{Al_2O_3} + \phi_{Cu})]^{2.5}}, \quad (25)$$

3. Numerical solution

The numerical simulation of the variations in temperatures per hour for the solar still system using an RL fractional operator is presented. Rewrite the model given by Eqs. (6)–(17) as

$${}^{RL}D_t^\alpha T = F(T), T(0) = T_0, 0 < \alpha \leq 1, \quad (26)$$

$$\begin{aligned} {}^{RL}D_t^\alpha T &= \begin{pmatrix} {}^{RL}D_t^\alpha T_g \\ {}^{RL}D_t^\alpha T_w \\ {}^{RL}D_t^\alpha T_p \end{pmatrix}, T = \begin{pmatrix} T_g \\ T_w \\ T_p \end{pmatrix}, T_0 = T_a, F(T) \\ &= \begin{pmatrix} f_1(t, T_g, T_w, T_p) \\ f_2(t, T_g, T_w, T_p) \\ f_3(t, T_g, T_w, T_p) \end{pmatrix}, \end{aligned}$$

where

$$f_1(t, T_g, T_w, T_p) = \omega_1 T_w - g_1 T_g + s_1 T_s + a_1 T_a + I_1(t),$$

$$f_2(t, T_g, T_w, T_p) = -\omega_2 T_w + g_2 T_g + p_1 T_p + I_2(t),$$

$$f_3(t, T_g, T_w, T_p) = -\omega_3 T_w + p_2 T_p + a_2 T_a + I_3(t),$$

and

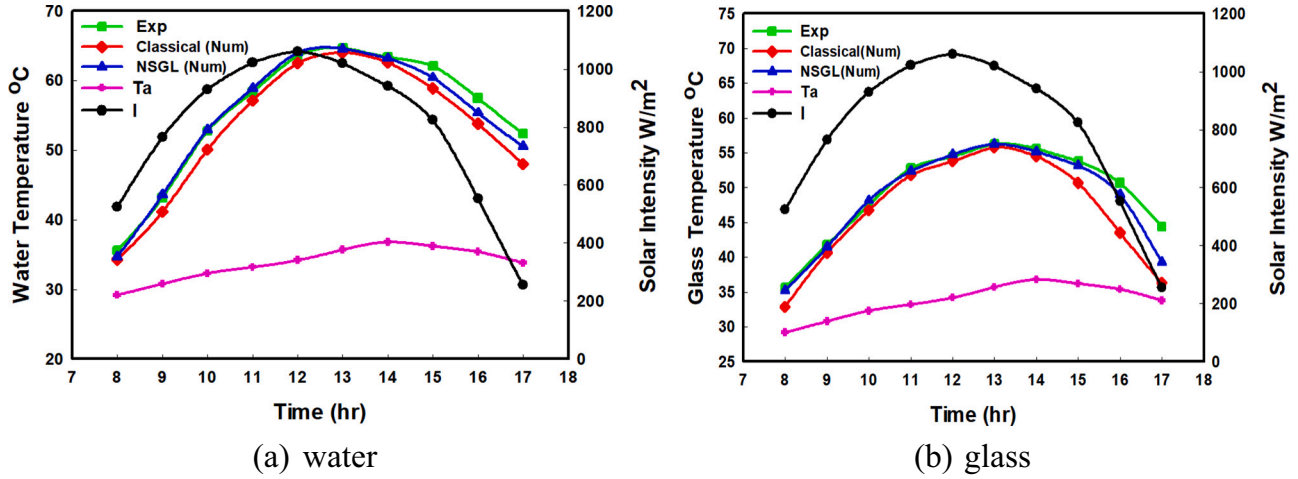


Fig. 3. Hourly variations of water and glass temperatures for classical derivative, NSGL, and experimental in summer.

$$\omega_1 = \frac{h_2 A_w}{m_g c_g}, g_1 = \frac{1}{m_g c_g} (h_2 A_w + h_{cg-a} A_g + h_{rg-s} A_g),$$

$$s_1 = \frac{h_{rg-s} A_g}{m_g c_g}, a_1 = \frac{h_{cg-a} A_g}{m_g c_g},$$

$$I_1(t) = \frac{\alpha_{eff,g} A_g}{m_g c_g} I(t), \omega_2 = \frac{1}{m_w c_w} (h_1 A_p + h_2 A_w),$$

$$g_2 = \frac{h_2 A_w}{m_w c_w}, p_1 = \frac{h_1 A_p}{m_w c_w}, I_2(t) = \frac{\alpha_{eff,w} A_w}{m_w c_w} I(t),$$

$$\omega_3 = \frac{1}{m_p c_p} (h_1 A_p), p_2 = \frac{1}{m_p c_p} (h_1 A_p - U_b A_p),$$

$$a_2 = \frac{1}{m_p c_p} (U_b A_p), I_3(t) = \frac{\alpha_{eff,p} A_p}{m_p c_p} I(t)$$

Now using the Definitions (1–4), we can discretize the system given by (26), as follows

$$T_{g,k} = \bar{\varphi}^\alpha f_1 (t_k, T_{g,k}, T_{w,k}, T_{p,k}) - \sum_{j=1}^k w_j^\alpha T_{g,k-j}, \quad (27)$$

$$T_{w,k} = \bar{\varphi}^\alpha f_2 (t_k, T_{g,k}, T_{w,k}, T_{p,k}) - \sum_{j=1}^k w_j^\alpha T_{w,k-j}, \quad (28)$$

$$T_{p,k} = \bar{\varphi}^\alpha f_3 (t_k, T_{g,k}, T_{w,k}, T_{p,k}) - \sum_{j=1}^k w_j^\alpha T_{p,k-j}, \quad (29)$$

where,  $w_j^\alpha$  and  $\bar{\varphi}^\alpha = (\varphi(h))^\alpha$  are given in Definition 4.

#### 4. Results and discussions

A new non-local model is presented to assess the SS performance utilizing nonstandard Grünwald-Letnikov (NSGL) and Grünwald-Letnikov (GL) approximation fractional operators, with order  $\alpha = 0.2$ . Also, a comparison between the new model and the classical model solved by using MATLAB utilizing RK4 is investigated. The input data for the solar radiation and the ambient temperature used in this analysis were measured in winter at 23/12/2017 and summer at 6/5/2017 [2]. Both the fractional and classical models for conventional SS are compared and validated with the experimental data published in [2].

##### 4.1. Comparison of numerical solution models

###### 4.1.1. Temperatures

Fig. 2a and b show the water and glass temperatures variation, respectively, in winter for the experimental results [2], using nonstandard Grünwald-Letnikov (NSGL) approximation fractional operator with order  $\alpha = 0.2$ , and classical model results. Also, the change of the solar

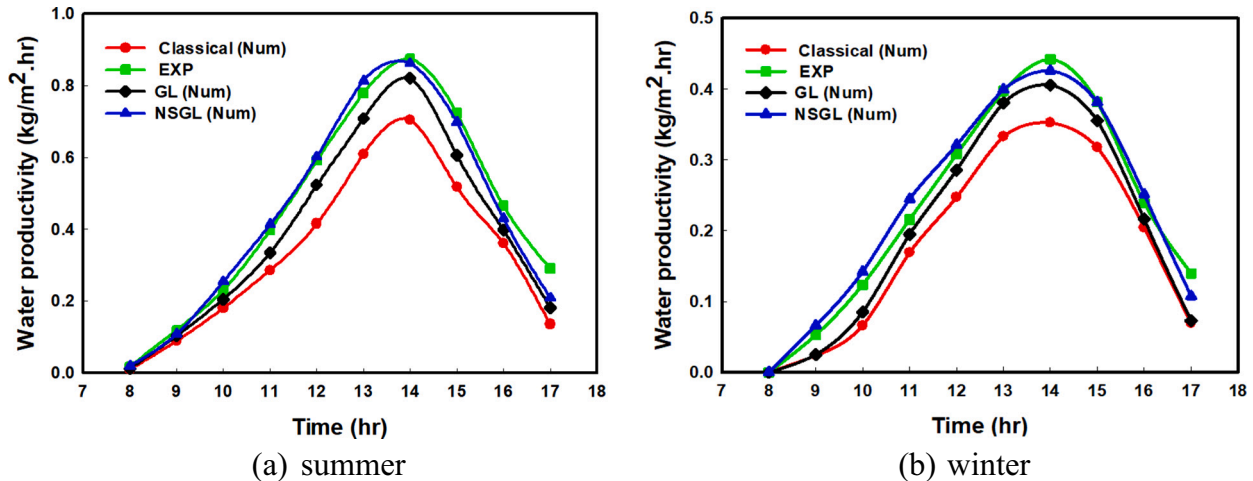


Fig. 4. Hourly variation of water productivity for classical derivative, GL, NSGL, and experimental.

intensity and surrounding temperature are superimposed on these figures. It is found that solar radiation increases from starting the measurements at 8 a.m. and reaches its maximum value at nearby 12 p.m. (solar noon) then declines gradually with time to the end of measuring time. The behavior of salty water temperature in Fig. 2a and glass temperature in Fig. 2b is because these temperatures of glass and brackish water take the same behavior of the solar radiation intensity. However, the value of the maximum temperature is achieved at approximately 1 p.m. The time lag between the greatest value of solar radiation intensity and the temperature is due to the time passes in heating the salty water and glass walls, etc. According to Fig. 2a, the hourly variation in water temperature using the NSGL operator has a perfect agreement with those of real experiments. This is because the fractional operator considers the non-local and non-singular kernel properties with a good memory effect. It can be seen that the maximum value of water temperature, according to NSGL is 47.54 °C. In comparison, the value of water temperature that was measured in the experiment is 47.46 °C. Unlike using the classical derivative (integer order), it is perceived that the greatest value of salty water temperature is 46.2 °C. This means that the percentage of relative error for saline water temperature is 2.65% using the classical derivative, but this percentage reduces to reach 0.168% using the NSGL operator. Similarly, as in water temperature, the numerical results using the NSGL operator have a good agreement according to those of the experiment for the glass temperature. It is found that at 1 p.m., the values of glass temperature are 33.89 °C and 35.26 °C using standard derivative and fractional derivative, respectively. In contrast, the value of glass temperature that results from the experiment is 35.24 °C at the same hour. This means that the relative error between the experimental result and the theoretical result is about 0.056% using the fractional derivative.

Fig. 3a and b present the same results as Fig. 2a and b, respectively but in the summer season. These figures show that the water and glass temperature in summer has approximately the same trend in winter with higher values due to the increase in the values of solar radiation. For example, the highest value of water temperature that results from the experiment is 64.7 °C, and this signifies that the value of water temperature in summer increases by about 17 °C comparing with its value in winter with an increase of about 35.8%. This higher value of water temperature, in Fig. 3a, because of the growth of the maximum radiation intensity from winter to summer by about 25%, which indicates that the efficiency of the SS in a hot climate (summer) is larger than in cold (winter) as will be realized later. According to Fig. 3a, the values of water temperature using the NSGL operator has a good consistent with the curve result from the experimental data. In contrast, it is observed the difference among the water temperature values calculated using standard derivative and the values of the experimental results. As can be seen in the same figure, the maximum values for brackish water temperature using NSGL and classical derivative are 47.54 °C and 46.2 °C, respectively, at 1 p.m. Based on Fig. 3b, it is detected that the maximum values of glass temperature are 33.89 °C using the standard derivative, 35.26 °C using NSGL, and 35.24 °C from the real experiment. These results indicate that the error that results from using the NSGL operator is smaller than the error using a classical derivative. It is also observed that the values of glass wall temperature that was measured experimentally have a perfect consistency with the numerical results using NSGL comparing with those values of the classical derivative curve.

#### 4.1.2. Productivity

The hourly variations for water yield of the traditional SS in winter and summer are presented in Fig. 4a and b, respectively. Fig. 4 displays that hourly yield takes the same trend as the water temperature in both summer and winter seasons described previously. However, the maximum value is achieved at about 2 p.m. (1 h later from the time of maximum water temperature). This time lag is due to time-consuming in condensation and evaporation of the water and collecting the freshwater outside the still. Fig. 4 clearly shows the good agreement between the

**Table 2**

Thermophysical properties of used nanoparticles.

| Nanomaterial type              | Density (kg/m <sup>3</sup> ) | Thermal conductivity (W/m K) | Specific heat coefficient (J/kg K) |
|--------------------------------|------------------------------|------------------------------|------------------------------------|
| Al <sub>2</sub> O <sub>3</sub> | 3600                         | 30                           | 880                                |
| CuO                            | 6000                         | 33                           | 551                                |

experimental data of water productivity that was measured in the two seasons (winter and summer) and the numerical results that are calculated using the NSGL derivative. It is found that the maximum value of water productivity at 2 p.m. for winter is 0.4057 kg/m<sup>2</sup>·h using GL fractional derivative, while this value of still productivity is 0.4260 kg/m<sup>2</sup>·h when using NSGL derivative at the same order. These values mean that the error that results from GL fractional derivative is greater than the error that results from NSGL fractional derivative.

Fig. 4b clearly shows that the maximum value of water productivity is doubled in summer compared with its value in the winter season which reaches 0.8748 kg/m<sup>2</sup>·h. This is due to the higher values of solar radiation in hot climate conditions. The value of productivity proves that the SS efficiency in winter is smaller than in summer. Similarly, as in the case of the winter season, it can be observed that the values of produced freshwater that are theoretically calculated using GL and NSGL fractional derivative are closer to the experimental values of the still productivity compared with the results obtained by the standard derivative. It is found that the highest value of freshwater productivity is 0.7050 kg/m<sup>2</sup>·h when using the standard derivative, and there is a perfect agreement with the experimental output data with a maximum value of water productivity is 0.8618 kg/m<sup>2</sup>·h in case of using NSGL operator. Furthermore, the maximum value that results due to using the GL fractional derivative at the same order is 0.8209 kg/m<sup>2</sup>·h. These values show that the percentage error due to applying NSGL is about 1.486%, in contrast to the error results from the GL operator is 6.161% and an error of 24.1% in case of using a standard derivative in summer. While these errors are 3.243% and 20.08%, respectively in winter. All the previous results of water, glass temperature, and water productivity indicate that using the fractional model is more consistent with the experimental work and gives less percentage of error comparing with the classical model. These accurate results are due to that the fractional derivatives do not take into account only local characteristics of the dynamics but consider the global evolution of the system.

#### 4.2. Impact of using hybrid nanofluid

One of the essential weaknesses of the SS is the low production rate of freshwater. Increasing the SS productivity passively can be accomplished by increasing the salty water evaporation rate of the saline water or the condition rate of the evaporated fresh water. Increasing the evaporation rate can be carried out by enhancing the heat transfer within the salty water in the SS basin. Hybrid nanofluid is one of the most important technique which can be used to improve the evaporation rate through enhancing the transfer of heat by varying the base fluid (saline water) properties and hence increases the distilled production rate. A mixing of nanoparticles of copper oxide (CuO) and alumina (Al<sub>2</sub>O<sub>3</sub>) at a concentration of 0.025% for each nanoparticle with the saline water is introduced in this study. The applied nanoparticles' properties are demonstrated in Table 2 [69,70]. According to the previous results, the best fractional modeling for the solar still system, which gives less error and is more consistent with the experimental data, is the NSGL fractional operator. So, all the results of this section are presented by using the NSGL fractional operator.

##### 4.2.1. Impact on temperatures

Increasing the saline water temperature enhances the evaporation of the saline water yielding an enhancement of the SS produced freshwater yield. Fig. 5a and b give a comparison between the hourly variation of



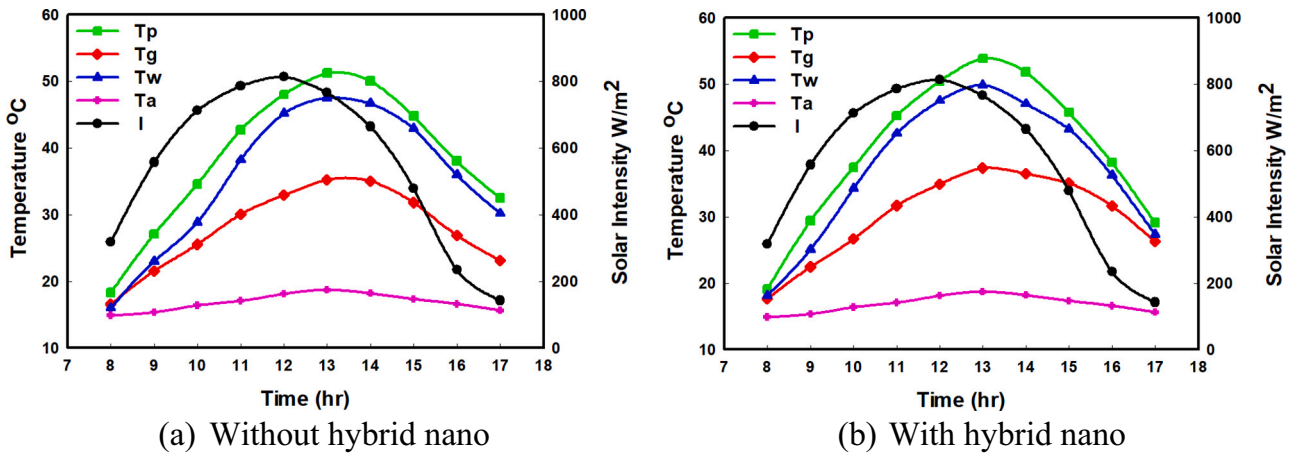


Fig. 5. Hourly variation of SS temperatures in winter with time.

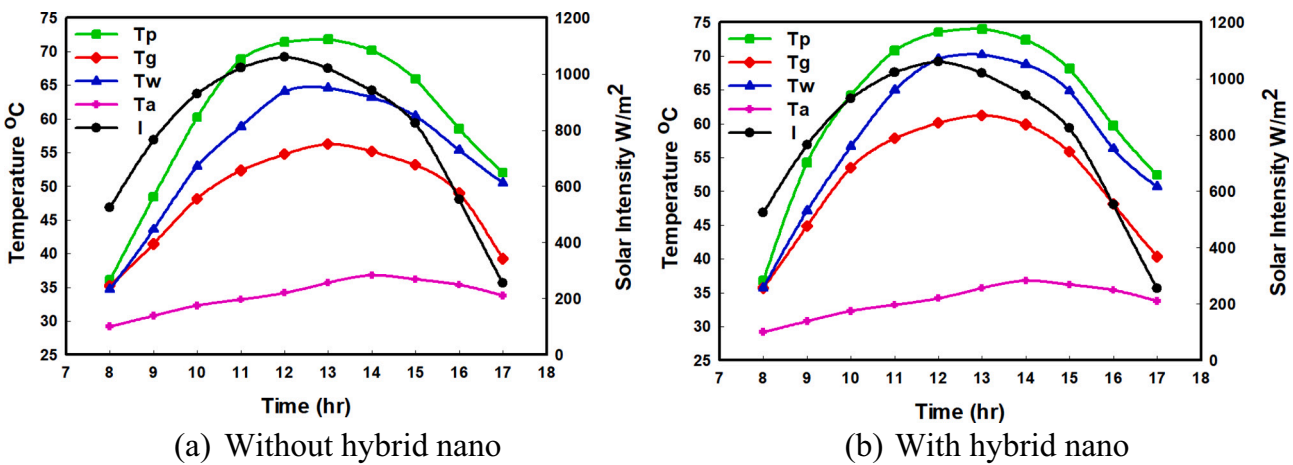


Fig. 6. Hourly variation of SS temperatures in summer with time.

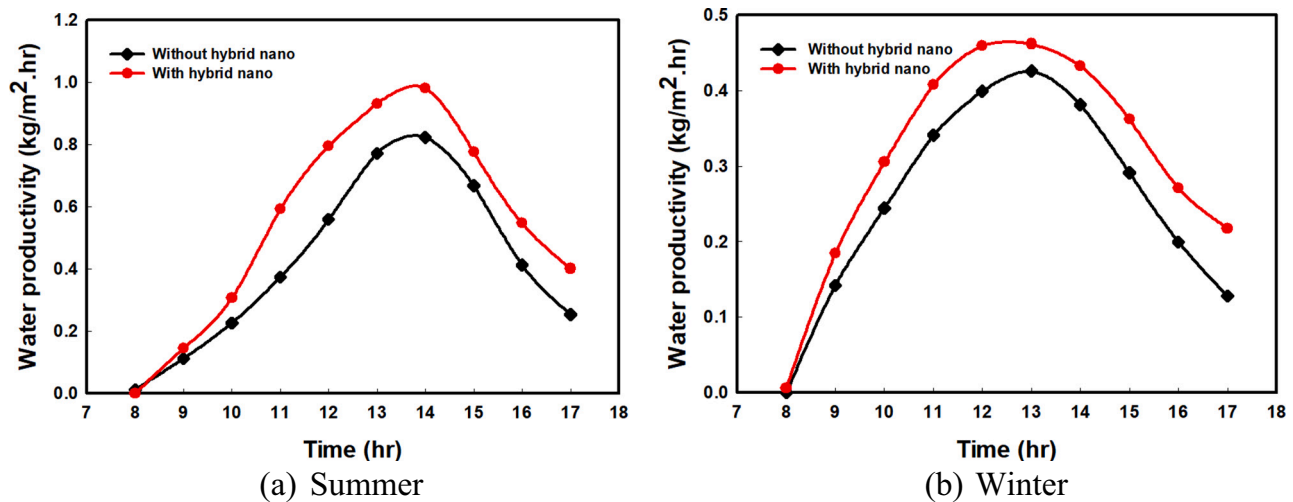


Fig. 7. Hourly variations of freshwater productivity with time.

the SS temperatures ( $T_g$ ,  $T_w$ ,  $T_p$ ) in winter with time without hybrid nano and with using hybrid nanofluid (saline water with hybrid nanoparticles), respectively. However, Fig. 6a and b show the same results of still temperatures, respectively but in the summer season. The solar

intensity and ambient temperature are superimposed on these figures for the measuring periods. It is clear from Figs. 5 and 6 that the trend of the solar still temperatures with using hybrid nano is the same as in the case of using the traditional fluid (salty water only). As shown in the two

**Table 3**  
Daily freshwater productivity.

| Daily productivity              | Without hybrid nano | With hybrid nano |
|---------------------------------|---------------------|------------------|
| Summer (kg/m <sup>2</sup> ·day) | 4.392               | 5.5239           |
| Winter (kg/m <sup>2</sup> ·day) | 2.553               | 3.1079           |

**Table 4**  
Comparison between the results of the present work and the literature studies on still productivity.

| Authors name           | Types of nanofluid  | Thermal conductivity (W/m K) | Water productivity (kg/m <sup>2</sup> ·day) |
|------------------------|---|------------------------------|---|
| Kabeel et al. [23]     | The cuprous (Cu <sub>2</sub> O)                           | 46                           | 2.240                                       |
| Kabeel et al. [23]     | The aluminum oxides (Al <sub>2</sub> O <sub>3</sub> )     | 76.5                         | 2.095                                       |
| Guptaa et al. [20]     | The copper oxide (CuO)                                    | 33.5                         | 3.058                                       |
| Sahota and Tiwari [71] | The aluminum oxides (Al <sub>2</sub> O <sub>3</sub> )     | 67.19                        | 2.665                                       |
| Subhedhar et al. [28]  | The aluminum oxides (Al <sub>2</sub> O <sub>3</sub> )     | 30                           | 1.741                                       |
| The present work       | Hybrid nanofluid (Al <sub>2</sub> O <sub>3</sub> and CuO) | 30                           | Summer<br>5.239                             |
|                        |   | 33                           | Winter<br>3.1079                            |

figures, if we compare the water temperatures, we can notice that the water temperature in the case of using hybrid nano is greater than without using hybrid nano, especially in summer; this is due to adding nanoparticles to the salty water improves the thermophysical properties of the base fluid, which raises the process of heat transfer especially in summer time and increases the values of temperature. For example, the maximum values of water temperature for only saline water are 47.5 and 64.6 °C in winter and summer, respectively, while in the case of using hybrid nano is 49.9 and 70.2 °C, respectively, with an increase of 5% and 8.7% in winter and summer seasons, respectively. Moreover, the highest value of glass temperature at 1 p.m. has risen from 56.29 °C to 61.26 °C in hot climate conditions after using the hybrid nanofluid. While, in cold conditions, the value of glass temperature has an increase of 2.5 °C.

#### 4.2.2. Impact on productivity

The foremost goal of the SS system is to yield fresh water from brackish water depending on the radiation from the sun. Fig. 7a and b

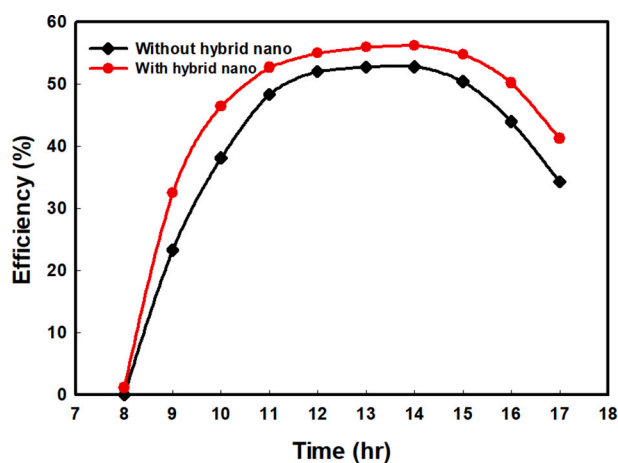
illustrate the hourly change of the produced freshwater productivity with time in summer and winter, respectively without and with hybrid nanofluid. Fig. 7 displays that the produced freshwater in summer is larger than winter due to the solar intensity and hence water temperature in summer is greater than winter as illustrated formerly. It is clear from Fig. 7 that using hybrid nanoparticles increases the SS productivity as compared to using only saline water where its maximum hourly value in winter and summer is 0.8618 and 0.426 kg/m<sup>2</sup>, respectively for only saline water and 0.9819 and 0.4618 kg/m<sup>2</sup>·h, respectively for saline water with hybrid nano. The reason behind this increment is the raising of the condensation and evaporation rate of the brackish water after using the hybrid nanofluid. The average daily freshwater productivity for the still with and without hybrid nano is listed in Table 3, which reveals that the daily productivity of the still with hybrid nano in summer and winter is 5.5239 and 3.1079 kg/m<sup>2</sup>·day, respectively with an excess of 27.2% and 21.7%, respectively as a contrast to still without hybrid nanoparticles. It is noted that the excess of the production of freshwater due to using nano in summer is larger than that in winter because the solar energy in summer is greater than in winter which enhances the influence of augmenting the heat transfer with the saline water due to using nanoparticles as stated previously. A comparison between the previous work and the present work to show the effect of using one type of nanofluid and using hybrid nanofluid on the productivity of SS is presented in Table 4. The results prove that there is a significant effect on the still productivity after using hybrid nanoparticles comparing with using one type only of nanoparticles.

#### 4.2.3. Impact on energy efficiency

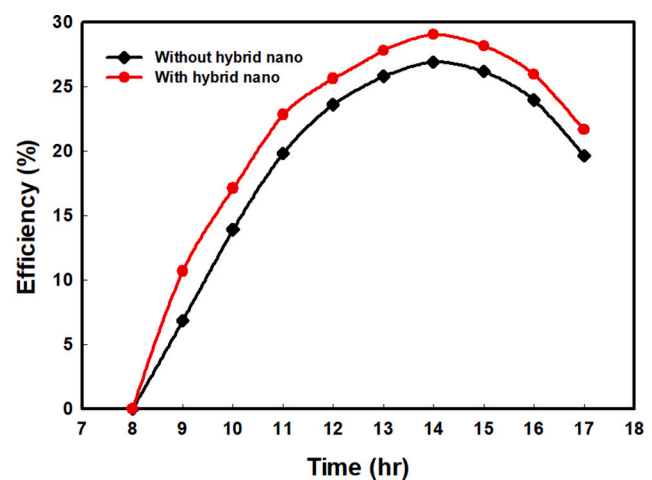
The hourly varying with time of energy efficiency without and with using hybrid nano in summer and winter are demonstrated in Fig. 8a and b, respectively. The findings show that energy efficiency augments with time from starting up at 8 a.m. to reach the maximum value at 2 p.m., and then it declines with time, as it has nearly the same trend as the still productivity curves. Additionally, as expected previously, the energy efficiency of the SS in winter is smaller than that in summer. Moreover, there is a significant impact on the solar still efficiency when using hybrid nanofluid. This change in the still efficiency is because hybrid

**Table 5**  
Average daily energy efficiency.

| Average energy efficiency | Without hybrid nano | With hybrid nano |
|---------------------------|---------------------|------------------|
| Summer                    | 44.013%             | 49.541%          |
| Winter                    | 20.751%             | 23.212%          |



(a) Summer



(b) winter

Fig. 8. Hourly variation of solar still efficiency with time.

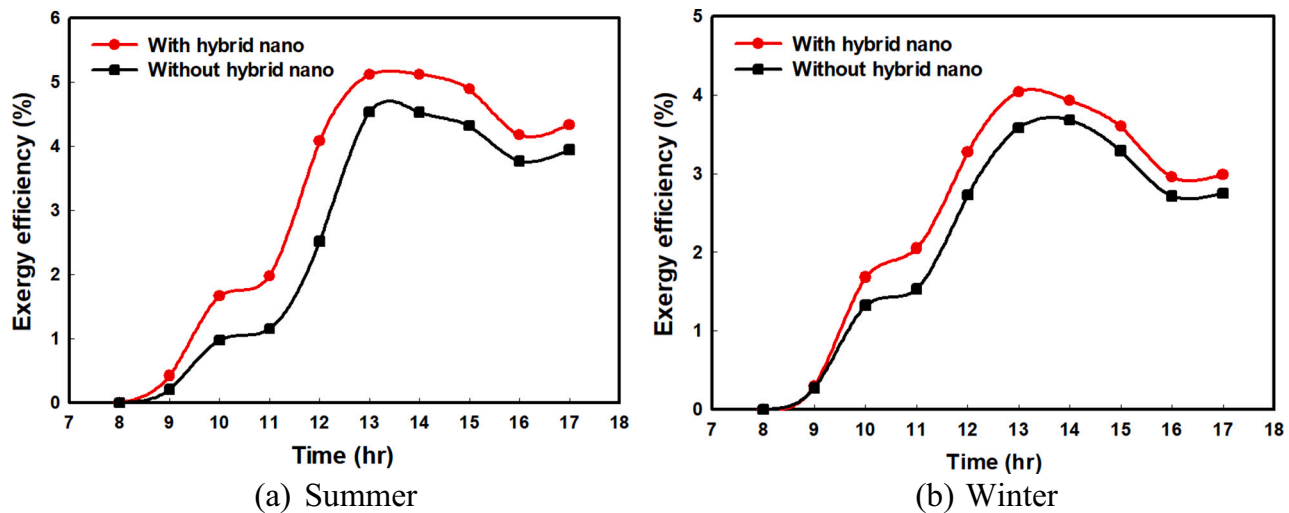


Fig. 9. Hourly variations of exergy efficiency with time.

**Table 6**  
Average daily exergy efficiency.

| Average exergy efficiency | Without hybrid nano | With hybrid nano |
|---------------------------|---------------------|------------------|
| Summer                    | 2.8848%             | 3.5325%          |
| Winter                    | 2.43%               | 2.756%           |

nanofluid raises the still productivity and hence increases its efficiency. The outcomes reveal that the maximum energy efficiency for the solar still without and with hybrid nano is about 52.81% and 56.16%, respectively in summer and 27.21 and 29.04%, respectively in winter with an increase of 6.7% and 6.3% in winter and summer. Table 5 displays the average daily SS energy efficiency without and with hybrid nano in summer and winter. Table 4 also shows that the maximum average efficiency is accomplished in the case of SS with a hybrid nanofluid of 49.54% in summer with an increase of 12.6% compared with still without nano while the increase due to using nano in winter is 11.85%.

#### 4.2.4. Impact on exergy efficiency

Exergy examination appears to be a powerful perception tool for the performance, design, optimization, and evaluation of any energy systems as compared to energy analysis, which is based on the first law of thermodynamics. The main importance of the exergy analysis is that the energy analysis only treats with energy conservation principles and doesn't provide knowledge on how much and where the performance of the system is degraded [57]. Contrarily, the exergy study provides a vision on the quality of energy and the potential usage of energy, and it is shown to be an efficient tool to determine the real magnitudes, locations, and types, of the irreversibilities and losses in the system procedures. Fig. 9a and b illustrate the hourly development of the exergy efficiency with time in summer and winter, respectively with and without using hybrid nanoparticles. According to Fig. 9 the exergy efficiency increases from the morning until about 2 p.m. and then it declines with time. It is obvious that the value of SS exergy efficiency is smaller than energy efficiency, which is stated in the previous section. The reason behind this behavior is, in exergy analysis, all system irreversibilities and losses are considered. Fig. 9 displays clearly that the exergy efficiency in the case of using hybrid nanoparticles is larger than the case without hybrid nanoparticles. Moreover, the impact of utilizing the nanoparticles on the wintertime is lesser than wintertime which is attributed to that the solar energy in summer is greater than winter as stated. The maximum exergy efficiency in summer is about 4.54% for traditional still (without nanoparticles) and increased to nearly 5.12%

after using nanoparticles, while these values in winter are 3.58 and 4.04%, respectively. The average daily exergy efficiency for studied systems is demonstrated in Table 6. The later reveals that using hybrid nanoparticles rises the exergy efficiency by nearby 22.5% in summer and 13.4% in winter, and this rising in the exergy efficiency is a result of raising the amount of freshwater productivity after using the hybrid nanofluid, as illustrated previously.

## 5. Conclusions

The effect of using hybrid nanoparticles of alumina and copper oxide ( $\text{Al}_2\text{O}_3\text{-CuO}$ ) on the performance of the solar still is studied numerically based on a new non-local model of two fractional operators: Grünwald-Letnikov and nonstandard Grünwald-Letnikov. A comparison between the numerical results of the fractional model and a classical model with experimental published data in hot (summer time) and cold (winter time) climate conditions of upper Egypt is also presented. The results show that the fractional model is more consistent with the real experiment than the classical model. It is also found that the NSGL fractional operator at order  $\alpha = 0.2$  is more consistent with the experimental data in the two seasons. It shows a percentage of error in the maximum value of water productivity reaches about 1.486% in summer and 3.423% in winter. Unlike the relative error that results from the classical derivative, which reaches nearly 19.4% and 20.08% in summer and winter, respectively. Based on the best fractional model, the results indicate that adding hybrid nanoparticles to the SS has a significant impact on the still in increasing the amount of freshwater production and improving both energy and exergy efficiency, and its impact in winter is lesser than in summer. It was found that using hybrid nanoparticles with the saline water of conventional single slope SS rises its output productivity by about 27.2% and 21.7%, in summer and winter, respectively. Furthermore, it increases its average daily efficiency to reach nearly 12.6% in summer and 11.85% in winter. Finally, mixing nanoparticles with saline water raises the average daily exergy efficiency of the SS by around 22.5% and 13.4% in hot and cold climate conditions, respectively. The impact of using hybrid-nano with passive and active solar still could be studied experimentally or theoretically.

#### CRediT authorship contribution statement

**E. F. El-Gazar:** Conceptualization, acquisition of data, analysis, writing original draft.

**W. K. Zahra:** Conceptualization, acquisition of data, design of the study, resources, interpretation of data, writing – review and editing.

**Hamdy Hassan:** Acquisition of data, Resources, Interpretation of data, reviewing and editing.

**Sherif I. Rabia:** Interpretation of data, reviewing.

### Declaration of competing interest

The authors declare no conflict of interest.

### Acknowledgment

E. F. El-Gazar acknowledges the support of the Missions Sector of the Ministry of Higher Education, Egypt through a Ph.D. scholarship.

### References

- H. Aghaei Zoori, F. Farshchi Tabrizi, F. Sarhaddi, F. Heshmatnezhad, Comparison between energy and exergy efficiencies in a weir type cascade solar still, *Desalination*. 325 (2013) 113–121, <https://doi.org/10.1016/j.desal.2013.07.004>.
- H. Hassan, Comparing the performance of passive and active double and single slope solar stills incorporated with parabolic trough collector via energy, exergy and productivity, *Renew. Energy* 148 (2020) 437–450, <https://doi.org/10.1016/j.renene.2019.10.050>.
- M. Fathy, H. Hassan, M. Salem Ahmed, Experimental study on the effect of coupling parabolic trough collector with double slope solar still on its performance, *Sol. Energy* 163 (2018) 54–61, <https://doi.org/10.1016/j.solener.2018.01.043>.
- H. Mousa, A.M. Gujarathi, Modeling and analysis the productivity of solar desalination units with phase change materials, *Renew. Energy* 95 (2016) 225–232, <https://doi.org/10.1016/j.renene.2016.04.013>.
- A. Elbar, H. Hassan, An experimental work on the performance of solar still incorporating with wind turbine and thermal energy storage unit, *Desalin. Water Treat.* 165 (2019) 24–34, <https://doi.org/10.5004/dwt.2019.24492>.
- R. Sathyamurthy, P.K. Nagarajan, Experimental investigations on conventional solar still with sand heat energy storage, *Int. J. Heat Technol.* 34 (2016) 597–603. doi:10.18280/ijht.340407.
- E. El-Bialy, M. Shalaby, An experimental investigation of a v-corrugated absorber single-basin solar still using PCM, *DES*. 398 (2016) 147–255.
- H. Panchal, K.K. Sadasivuni, M. Suresh, S. Yadav, Performance analysis of evacuated tubes coupled solar still with double basin solar still and solid fins, *Int. J. Ambient Energy*. 0 (2018) 1–16. doi:<https://doi.org/10.1080/01430750.2018.1501745>.
- M. Elashmawy, Improving the performance of a parabolic concentrator solar tracking-tubular solar still (PCST-TSS) using gravel as a sensible heat storage material, *Desalination*. 473 (2020) 114182, <https://doi.org/10.1016/j.desal.2019.114182>.
- M. Naroei, F. Sarhaddi, F. Sobhnamayan, Efficiency of a photovoltaic thermal stepped solar still: experimental and numerical analysis, *Desalination*. 441 (2018) 87–95, <https://doi.org/10.1016/j.desal.2018.04.014>.
- A.R. Abd Elbar, M.S. Yousef, H. Hassan, Energy, exergy, exergoeconomic and enviroeconomic (4E) evaluation of a new integration of solar still with photovoltaic panel, *J. Clean. Prod.* 233 (2019) 665–680, <https://doi.org/10.1016/j.jclepro.2019.06.111>.
- H. Panchal, R. Sathyamurthy, Experimental analysis of single basin solar still with porous fins, *Int. J. Ambient Energy*. 0 (2017) 1–15. doi:<https://doi.org/10.1080/01430750.2017.1360206>.
- S.M. Parsa, D. Javadi Y, A. Rahbar, M. Majidniya, M. Salimi, Y. Amidpour, M. Amidpour, Experimental investigation at a summit above 13,000 ft on active solar still water purification powered by photovoltaic: a comparative study, *Desalination*. 476 (2020) 114146. doi:<https://doi.org/10.1016/j.desal.2019.114146>.
- M. Elkelay, S.E. din H. Etaiw, H.A.E. Bastawissi, H. Marie, A. Elbanna, H. Panchal, K. Sadasivuni, H. Bhargav, Study of diesel-biodiesel blends combustion and emission characteristics in a CI engine by adding nanoparticles of Mn (II) supramolecular complex, *Atmos. Pollut. Res.* 11 (2020) 117–128. doi:<https://doi.org/10.1016/j.apr.2019.09.021>.
- M. Vaka, R. Walvekar, A.K. Rasheed, M. Khalid, H. Panchal, A review: emphasizing the nanofluids use in PV/T systems, *IEEE Access*. 8 (2020) 58227–58249, <https://doi.org/10.1109/ACCESS.2019.2950384>.
- H. Panchal, R. Sathyamurthy, A.E. Kabeel, S.A. El-Agouz, Ds.S. Rufus, T. Arunkumar, A. Muthu Manokar, D.P. Winston, A. Sharma, N. Thakar, K.K. Sadasivuni, Annual performance analysis of adding different nanofluids in stepped solar still, *J. Therm. Anal. Calorim.* 138 (2019) 3175–3182. doi:<https://doi.org/10.1007/s10973-019-08346-x>.
- R. Sathyamurthy, A.E. Kabeel, E.S. El-Agouz, Ds. Rufus, H. Panchal, T. Arunkumar, A.M. Manokar, D.P. Winston, Experimental investigation on the effect of MgO and TiO<sub>2</sub> nanoparticles in stepped solar still, *Int. J. Energy Res.* 43 (2019) 3295–3305. doi:<https://doi.org/10.1002/er.4460>.
- A.E. Kabeel, R. Sathyamurthy, S.W. Sharshir, A. Muthumanokar, H. Panchal, N. Prakash, C. Prasad, S. Nandakumar, M.S. El Kady, Effect of water depth on a novel absorber plate of pyramid solar still coated with TiO<sub>2</sub> nano black paint, *J. Clean. Prod.* 213 (2019) 185–191, <https://doi.org/10.1016/j.jclepro.2018.12.185>.
- A.E. Kabeel, Z.M. Omara, F.A. Essa, Improving the performance of solar still by using nanofluids and providing vacuum, *Energy Convers. Manag.* 86 (2014) 268–274, <https://doi.org/10.1016/j.enconman.2014.05.050>.
- B. Gupta, P. Shankar, R. Sharma, P. Baredar, Performance enhancement using nano particles in modified passive solar still, *Procedia Technol.* 25 (2016) 1209–1216, <https://doi.org/10.1016/j.protcy.2016.08.208>.
- S.M. Parsa, A. Rahbar, M.H. Koleini, Y. Davoud Javadi, M. Afrand, S. Rostami, M. Amidpour, First approach on nanofluid-based solar still in high altitude for water desalination and solar water disinfection (SODIS), *Desalination*. 491 (2020) 114592, <https://doi.org/10.1016/j.desal.2020.114592>.
- L. Sahota, S. Arora, H.P. Singh, G. Sahoo, Thermo-physical characteristics of passive double slope solar still loaded with MWCNTs and Al<sub>2</sub>O<sub>3</sub>-water based nanofluid, *Mater. Today Proc.* (2020) 1–6, <https://doi.org/10.1016/j.matpr.2020.01.600>.
- A.E. Kabeel, Z.M. Omara, F.A. Essa, Numerical investigation of modified solar still using nanofluids and external condenser, *J. Taiwan Inst. Chem. Eng.* 75 (2017) 77–86, <https://doi.org/10.1016/j.jtice.2017.01.017>.
- S. Rashidi, M. Bovand, N. Rahbar, J. Abolfazli, Steps optimization and productivity enhancement in a nanofluid cascade solar still, *Renew. Energy* 118 (2018) 536–545, <https://doi.org/10.1016/j.renene.2017.11.048>.
- M. Al-harashsheh, M. Abu-Arabi, H. Mousa, Z. Alzghoul, Solar desalination using solar still enhanced by external solar collector and PCM, *Appl. Therm. Eng.* 128 (2018) 1030–1040.
- S. Rashidi, S. Akar, M. Bovand, R. Ellahi, Volume of fluid model to simulate the nano fluid flow and entropy generation in a single slope solar still 115 (2018) 400–410, <https://doi.org/10.1016/j.renene.2017.08.059>.
- O. Bait, M.S. Ameer, Enhanced heat and mass transfer in solar stills using nanofluids: a review, *Sol. Energy* 170 (2018) 694–722, <https://doi.org/10.1016/j.solener.2018.06.020>.
- D.G. Subhedar, K. V Chauhan, K. Patel, B.M. Ramani, Improvement of a conventional single slope single basin passive solar still by integrating with nanofluid-based parabolic trough collector: an experimental study, *Mater. Today Proc.* (2020) 2–5. doi:<https://doi.org/10.1016/j.matpr.2020.02.304>.
- T.R. Shah, Applications of hybrid nano fluid in solar energy, practical limitations and challenges: a critical review, 183 (2019) 173–203.
- X. Li, G. Zeng, X. Lei, Solar Energy Materials and Solar Cells The stability, optical properties and solar-thermal conversion performance of SiC-MWCNTs hybrid nanofluids for the direct absorption solar collector (DASC) application, *Sol. Energy Mater. Sol. Cells* 206 (2020) 110323. doi:<https://doi.org/10.1016/j.solmat.2019.110323>.
- M. Vaka, R. Walvekar, M. Khalid, P. Jagadish, N.M. Mubarak, H. Panchal, Synthesis of hybrid graphene/TiO<sub>2</sub> nanoparticles based high-temperature quinary salt mixture for energy storage application, *J. Energy Storage*. 31 (2020) 101540, <https://doi.org/10.1016/j.est.2020.101540>.
- R.K. Bumataria, N.K. Chavda, H. Panchal, Current research aspects in mono and hybrid nanofluid based heat pipe technologies, *Heliyon*. 5 (2019), e01627, <https://doi.org/10.1016/j.heliyon.2019.e01627>.
- A. Adriana, W.M. El-maghlany, Influence of hybrid nano fluids on the performance of parabolic trough collectors in solar thermal systems: recent findings and numerical comparison 120 (2018) 350–364.
- E.C. Okonkwo, I. Wole-oshio, D. Kavaz, M. Abid, T. Al-ansari, Thermodynamic evaluation and optimization of a flat plate collector operating with alumina and iron mono and hybrid nanofluids, *Sustain. Energy Technol. Assessments*. 37 (2020) 100636, <https://doi.org/10.1016/j.seta.2020.100636>.
- S. Kumar, A. Kumar, S. Tiwari, D. Singh, Performance analysis of hybrid nano fluids in flat plate solar collector as an advanced working fluid 167 (2018) 231–241.
- S. Maitama, Local fractional natural homotopy perturbation method for solving partial differential equations with local fractional derivative, *Prog. Fract. Differ. Appl.* 4 (2018) 219–228.
- W. Mitkowski, J. Kacprzyk, J. Baranowski, *Advances in the Theory and Applications of Non-integer Order Systems* (2013), <https://doi.org/10.1007/978-3-319-00933-9>.
- V. Suat, S. Momani, Solving systems of fractional differential equations using differential transform method, *J. Comput. Appl. Math.* 14 (2008) 142–151.
- C.F. Lorenzo, T.T. Hartley, Initialization, conceptualization, and application in the generalized (fractional) calculus, *Crit. Rev. Biomed. Eng.* 35 (2007) 447–553, <https://doi.org/10.1615/CritRevBiomedEng.v35.i6.10>.
- A.A. Kilbas, H.M. Srivastava, J.J. Trujillo, *Theory and Applications of Fractional Differential Equations*, 2006.
- L. Ouhssaine, Y. Boukal, M. El Ganoui, A general fractional-order heat transfer model for photovoltaic/thermal hybrid systems and its observer design, *Energy Procedia* 139 (2017) 49–54, <https://doi.org/10.1016/j.egypro.2017.11.171>.
- K.M. Owolabi, Mathematical modelling and analysis of love dynamics: a fractional approach, *Phys. A Stat. Mech. Its Appl.* 525 (2019) 849–865, <https://doi.org/10.1016/j.physa.2019.04.024>.
- M.A. Akinlar, A. Cevikel, Efficient solutions of systems of fractional PDEs by the differential transform method, *Adv. Differ. Equations*. 188 (2012) 1–7.
- M.I. Tropicarevsky, S.A. Seminara, A. Marcela, A review on fractional differential equations and a numerical method to solve some boundary value problems, *Intech i 13* (2012), <https://doi.org/10.1016/j.colsurfa.2011.12.014>.
- M. Caputo, M. Fabrizio, Applications of new time and spatial fractional derivatives with exponential kernels, *Progr. Fract. Differ. Appl.* 2 (2016) 1–11.
- K.M. Owolabi, A. Atangana, On the formulation of adams-bashforth scheme with atangana-baleanu-caputo fractional derivative to model chaotic problems, *Chaos*. 29 (2019). doi:<https://doi.org/10.1063/1.5085490>.

- [47] R. Khalil, A new definition of fractional derivative, *J. Comput. Appl. Math.* 264 (2014) 65–70.
- [48] W.K. Zahra, M.A. Nasr, M. Van Daele, Exponentially fitted methods for solving time fractional nonlinear reaction-diffusion equation, *Appl. Math. Comput.* 358 (2019) 468–490.
- [49] A.D. Obembe, M.E. Hossain, S.A. Abu-Khamsin, Variable-order derivative time fractional diffusion model for heterogeneous porous media, *J. Pet. Sci. Eng.* 152 (2017) 391–405, <https://doi.org/10.1016/j.petrol.2017.03.015>.
- [50] M. Žecová, J. Terpák, Heat conduction modeling by using fractional-order derivatives, *Appl. Math. Comput.* 257 (2015) 365–373, <https://doi.org/10.1016/j.amc.2014.12.136>.
- [51] W.K. Zahra, M.A. Nasr, Exponentially fitted methods for solving two dimensional time fractional damped Klein–Gordon equation with nonlinear source term, *Commun. Nonlinear Sci. Numer. Simul.* 73 (2019) 177–194.
- [52] D. Sierociuk, T. Skovranek, M. Macias, A.D. Igor Podlubny, P. Ziubinski, Diffusion process modeling by using fractional-order models, *Appl. Math. Comput.* 257 (2015) 2–11, <https://doi.org/10.1016/j.amc.2014.11.028>.
- [53] W.K. Zahra, M. Abdel-aty, D. Abidou, A fractional model for estimating the hole geometry in the laser drilling process of thin metal sheets, *Chaos, Solitons Fractals Interdiscip. J. Nonlinear Sci. Nonequilibrium Complex Phenom.* 136 (2020) 109843, <https://doi.org/10.1016/j.chaos.2020.109843>.
- [54] G. Sales Teodoro, J.A. Tenreiro Machado, E. Capelas de Oliveira, A review of definitions of fractional derivatives and other operators, *J. Comput. Phys.* 388 (2019) 195–208, <https://doi.org/10.1016/j.jcp.2019.03.008>.
- [55] H. Sun, A. Chang, Y. Zhang, W. Chen, A review on variable-order fractional differential equations: mathematical foundations, physical models, numerical methods and applications, *Fract. Calc. Appl. Anal.* 22 (2019) 27–59, <https://doi.org/10.1515/fca-2019-0003>.
- [56] R. Garrappa, E. Kaslik, M. Popolizio, Evaluation of fractional integrals and derivatives of elementary functions: overview and tutorial, *Mathematics.* 7 (2019) 1–21, <https://doi.org/10.3390/math7050407>.
- [57] M.S. Yousef, H. Hassan, M. Ahmed, S. Ookawara, Energy and exergy analysis of single slope passive solar still under Egyptian climate conditions, *Energy Procedia.* 141 (2017) 18–23. doi:<https://doi.org/10.1016/j.egypro.2017.11.005>.
- [58] H. Hassan, M.S. Ahmed, M. Fathy, M.S. Yousef, Impact of salty water medium and condenser on the performance of single acting solar still incorporated with parabolic trough collector, *Desalination.* 480 (2020). doi:<https://doi.org/10.1016/j.desal.2020.114324>.
- [59] M.S. Yousef, H. Hassan, Assessment of different passive solar stills via exergoeconomic, exergoenvironmental, and exergoenvironmental approaches: a comparative study, *Sol. Energy* 182 (2019) 316–331. doi:<https://doi.org/10.1016/j.solener.2019.02.042>.
- [60] A.R. Abd Elbar, H. Hassan, Experimental investigation on the impact of thermal energy storage on the solar still performance coupled with PV module via new integration, *Sol. Energy* 184 (2019) 584–593, <https://doi.org/10.1016/j.solener.2019.04.042>.
- [61] A.A. Hawwash, A.K. Abdel-Rahman, S. Ookawara, S.A. Nada, Experimental study of alumina nanofluids effects on thermal performance efficiency of flat plate solar collectors, *Int. J. Eng. Technol.* 4 (2016) 123–131, <https://doi.org/10.5176/2251-3701>.
- [62] A.A. Hawwash, A.K. Abdel Rahman, S.A. Nada, S. Ookawara, Numerical investigation and experimental verification of performance enhancement of flat plate solar collector using nanofluids, *Appl. Therm. Eng.* 130 (2018) 363–374, <https://doi.org/10.1016/j.applthermaleng.2017.11.027>.
- [63] M. Sahooji, S. Sabbaghi, CuO nanofluids: the synthesis and investigation of stability and thermal conductivity, *J. Nanofluids.* 1 (2013) 155–160, <https://doi.org/10.1166/jon.2012.1014>.
- [64] L. Yang, W. Jiang, A new thermal conductivity model for nanorod-based nanofluids, *Appl. Therm. Eng.* 114 (2017) 287–299.
- [65] H. Hassan, S. Harmand, 3D transient model of vapour chamber: effect of nanofluids on its performance, *Appl. Therm. Eng.* 51 (2013) 1191–1201, <https://doi.org/10.1016/j.applthermaleng.2012.10.047>.
- [66] S.M. Aminossadati, B. Ghasemi, Natural convection cooling of a localised heat source at the bottom of a nanofluid-filled enclosure, *Eur. J. Mech. B, Fluids.* 28 (2009) 630–640.
- [67] H. Hassan, Heat transfer of Cu-water nanofluid in an enclosure with a heat sink and discrete heat source, *Eur. J. Mech. B/Fluids.* 45 (2014) 72–83, <https://doi.org/10.1016/j.euromechflu.2013.12.003>.
- [68] G.C. Bourantas, V.C. Loukopoulos, Modeling the natural convective flow of micropolar nanofluids, *Int. J. Heat Mass Transf.* 68 (2014) 35–41.
- [69] S.M. Murshed, K.C. Leong, C. Yang, Thermophysical and electrokinetic properties of nanofluids – a critical review, *Appl. Therm. Eng.* 28 (2008) 2109–2152.
- [70] M. Saqib, I. Khan, S. Shafie, Application of fractional differential equations to heat transfer in hybrid nanofluid: modeling and solution via integral transforms, *Adv. Differ. Equations.* 2019 (2019) 763–769, <https://doi.org/10.1186/s13662-019-1988-5>.
- [71] L. Sahota, G.N. Tiwari, ScienceDirect effect of Al<sub>2</sub>O<sub>3</sub> nanoparticles on the performance of passive double slope solar still, *Sol. Energy* 130 (2016) 260–272, <https://doi.org/10.1016/j.solener.2016.02.018>.